

Giant Spin Lifetime Anisotropy and Spin-Valley Locking in Silicene and Germanene from First-Principles Density-Matrix Dynamics

Junqing Xu,[†] Hiroyuki Takenaka,[†] Adela Habib,[‡] Ravishankar Sundararaman,^{*,¶}
and Yuan Ping^{*,†}

[†]*Department of Chemistry and Biochemistry, University of California, Santa Cruz, CA 95064, USA*

[‡]*Department of Physics, Applied Physics and Astronomy, Rensselaer Polytechnic Institute, 110 8th Street, Troy, New York 12180, USA*

[¶]*Department of Materials Science and Engineering, Rensselaer Polytechnic Institute, 110 8th Street, Troy, New York 12180, USA*

E-mail: sundar@rpi.edu; yuanping@ucsc.edu

Abstract

Through First-Principles real-time Density-Matrix (FPDM) dynamics simulations, we investigate spin relaxation due to electron-phonon and electron-impurity scatterings with spin-orbit coupling in two-dimensional Dirac materials - silicene and germanene, at finite temperatures and under external fields. We discussed the applicability of conventional descriptions of spin relaxation mechanisms by Elliott-Yafet (EY) and D'yakonov-Perel' (DP) compared to our FPDM method, which is determined by a complex interplay of intrinsic spin-orbit coupling, external fields, and electron-phonon coupling strength, beyond crystal symmetry. For example, the electric field dependence of spin relaxation time is close to DP mechanism for silicene at room temperature, but rather similar to EY mechanism for germanene. Due to its stronger spin-orbit coupling strength and buckled structure in sharp contrast to graphene, germanene has a giant spin lifetime anisotropy and spin valley locking effect under nonzero E_z and relatively low temperature. More importantly, germanene has extremely long spin lifetime (~ 100 ns at 50 K) and ultrahigh carrier mobility, which makes it advantageous for spin-valleytronic applications.

Introduction

Shortly after the discovery of graphene, significant advances have been made in the field of spintronics, exploiting spin transport instead of charge transport, with much less dissipation and unprecedented potentials for low-power electronics. Several properties are key parameters for optimizing spin transport, such as long spin lifetime and diffusion length, high

electronic mobility, spin-valley locking effect. Long spin lifetime and diffusion length ensure robust spin state during propagation in a device. The spin-valley locking effect is valuable for the emerging field of research - "valleytronics",¹⁻³ which utilizes the valley-pseudospin degree of freedom as basic unit for quantum information technology.

Graphene is a very promising spintronic material⁴, in particular, with the extremely high electronic mobility⁵ and the longest known spin

diffusion length at room temperature⁶. However, due to its weak spin-orbit coupling (SOC), spin-valley locking effect may be realized only through external effects, e.g., through proximity effect - by interfacing with large SOC materials such as transition metal dichalcogenides (TMDs)^{7,8}. Other 2D materials⁹ including TMDs¹⁰ have also shown exciting properties for spin-/valley-tronics.¹⁻³ For instance, in Ref. 10, the ultralong spin/valley lifetime is observed (e.g. 2 μ s in p-type monolayer WSe₂ at 5 K) and the spin lifetime is insensitive to in-plane magnetic fields, which is a signature of the spin-valley locking effects. However, in general, TMDs have much lower electric mobility than graphene^{11,12}, which is not ideal for electronic device applications.

As the counterparts of graphene, silicene and germanene have attracted significant attention throughout a decade due to their resemblance and distinction from graphene¹³⁻¹⁷. They possess several remarkable properties, including gate-tunable carrier concentration, high electric mobility^{18,19} (Fig. S8), quantum spin hall effects^{20,21}, etc. Moreover, due to the buckled geometry, their SOC strength is highly enhanced and they will also have the advantages of tunable band structures by applying perpendicular electric fields E_z and high spin polarizations, which are promising for spintronic applications¹⁴. Their electronic structure under finite E_z has similarity to those of TMDs: the signs of spins in K and K' valleys being opposite which is imposed by time-reversal symmetry, band splittings induced by SOC and highly polarized states. Therefore, silicene and germanene can combine the advantages of both graphene and TMDs but avoid some shortcomings such as limited spin lifetimes (\leq tens of ns) in graphene samples,^{22,23} the absence of spin-valley locking in graphene, and low mobilities in TMDs^{11,12}.

Despite of their promising properties, the potential for spin-based information technologies by silicene and germanene has yet to be demonstrated. Understanding spin dynamics and transport in materials is of key importance for spintronics and spin-based quantum information science, and one key metric of useful spin

dynamics is spin lifetime τ_s . Compared with graphene, of which τ_s has been extensively studied experimentally and theoretically^{6,25,26}, τ_s of silicene and germanene have not been measured and the existing few theoretical studies were done based on relatively simple models^{27,28}, which do not include realistic interactions with phonons and impurities. Recently we developed a First-Principles Density-Matrix (FPDM) approach with quantum descriptions of scattering processes between electron-phonon (e-ph), electron-impurities (e-i) and electron-electron, to simulate spin-orbit mediated spin dynamics in general solid-state systems with arbitrary symmetry^{29,30}. By employing this new method, we will be able to predict τ_s of silicene and germanene at finite temperatures with realistic interactions with environment without introducing any simplified model or empirical parameters, for ps to μ s timescale simulation.

Results and discussions

Electronic structure. We first show electronic quantities of silicene and germanene under different E_z , which are closely related to spin dynamics and essential for understanding spin relaxation mechanisms.

Fig. 1(a) describes a schematic picture of band structures under E_z . DFT results of band gaps and the average of band splittings $\langle\Delta\rangle$ between two conduction/valence bands (broken Kramers' degeneracy under E_z field) are shown in Fig. 1(c). ' $\langle\rangle$ ' represents taking average of electronic quantity A by²⁴ $\langle A \rangle = \sum_{kn} f'(\epsilon_{kn}) A_{kn} / \sum_{kn} f'(\epsilon_{kn})$, where f' is the derivative of Fermi-Dirac distribution function, and k and n are k-point and band indices respectively. At $E_z = 0$, due to time-reversal and inversion symmetries, every two bands form a Kramers degenerate pair.³¹ A finite E_z splits a Kramers pair into spin-up and spin-down bands due to broken inversion symmetry and the splitting increases with E_z (see Fig.1(c)). As the earlier model Hamiltonian study¹³ presented, the phase transition from topological insulators to band insulators happens at the critical electric field E_{cr} with the schematic band struc-

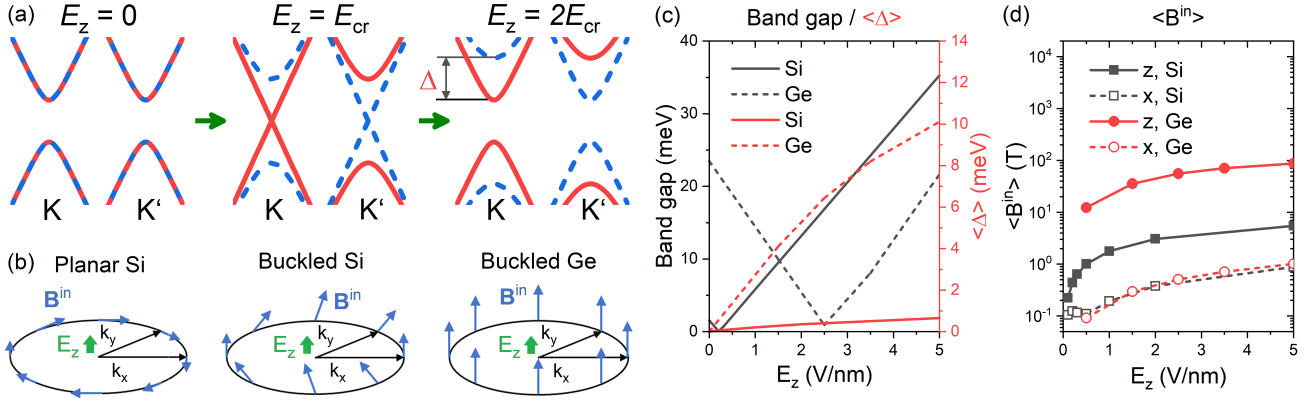


Figure 1: Electronic quantities of silicene and germanene under different perpendicular electric field (E_z). (a) The schematic diagrams of band structures of silicene and germanene under different E_z (see calculated band structures in Fig. S3-S5), where E_{cr} is the critical electric field leading to zero band gap. (b) The schematic diagrams of internal magnetic fields \mathbf{B}^{in} (blue arrows) at a Fermi circle near one Dirac cone of planar silicene, (buckled) silicene, (buckled) germanene induced by breaking inversion symmetry under finite E_z . $\mathbf{B}_{kn}^{\text{in}} = 2\Delta_{kn}\mathbf{S}_{kn}^{\text{exp}} / (g_e\mu_B)$, where k and n are k -point and band indices, respectively. $g_e\mu_B$ is the electron spin gyromagnetic ratio. Δ_{kn} is energy difference between two conduction (valence) bands when n is a conduction (valence) band. \mathbf{S}^{exp} is a vector and $\mathbf{S}^{\text{exp}} \equiv (S_x^{\text{exp}}, S_y^{\text{exp}}, S_z^{\text{exp}})$, where S_i^{exp} is spin expectation value along direction i and is the diagonal element of spin matrix s_i in Bloch basis. (c) Band gaps (black lines) and the averaged band splitting energies $\langle \Delta \rangle$ (red lines) between two conduction/valence bands. (d) The averaged out-of-plane (B_z^{in}) and in-plane internal magnetic fields (B_x^{in}). Throughout this work, $\langle A \rangle$ means the average²⁴ of electronic quantity A and $\langle A \rangle = \sum_{kn} f'(\varepsilon_{kn}) A_{kn} / \sum_{kn} f'(\varepsilon_{kn})$. f' is the derivative of Fermi-Dirac distribution function. In this figure, for averaging, $T = 300$ K and chemical potential μ is set in the middle of the band gap.

tures shown in Fig. 1(a). Based on our DFT calculations, the band gaps close in silicene and germanene (black solid and dashed lines in Fig. 1(c)) at 0.2 and 2.5 V/nm respectively, and the gaps open again above E_{cr} .

The band splittings between spin-up and down under a finite E_z are effectively induced by k - and band-dependent “internal” magnetic fields \mathbf{B}^{in} , which are SOC fields induced by broken inversion symmetry.³¹ \mathbf{B}^{in} is defined as $2\Delta_{kn}\mathbf{S}_{kn}^{\text{exp}} / (g_e\mu_B)$, $g_e\mu_B$ is the electron spin gyromagnetic ratio. $\mathbf{S}^{\text{exp}} \equiv (S_x^{\text{exp}}, S_y^{\text{exp}}, S_z^{\text{exp}})$, where S_i^{exp} is spin expectation value along direction i and is the diagonal element of spin matrix s_i in Bloch basis.

In Fig. 1(b), we depict schematic diagrams of \mathbf{B}^{in} (blue arrows) on a Fermi circle near one Dirac cone of planar silicene, buckled silicene, and buckled germanene induced by finite E_z . In planar silicene, \mathbf{B}^{in} is purely in-plane, known as Rashba Spin-Orbit fields \mathbf{B}_R^{in} .

\mathbf{B}^{in} in buckled silicene is analogous to an admixture of \mathbf{B}_R^{in} and out-of-plane field B_z^{in} , because buckled geometry results in the presence of B_z^{in} . Different from silicene, \mathbf{B}^{in} in buckled germanene is nearly fully out-of-plane. This indicates that stronger intrinsic SOC in germanene significantly increases out-of-plane B_z^{in} and, as a result, the proportion of in-plane component diminishes. We examine the averaged B^{in} along z , $\langle B_z^{\text{in}} \rangle$, and along x , $\langle B_x^{\text{in}} \rangle$, under E_z shown in Fig.1(d). While $\langle B_x^{\text{in}} \rangle$ for silicene and germanene increase slowly with similar values, $\langle B_z^{\text{in}} \rangle$, for germanene due to stronger intrinsic SOC, rises much more rapidly than that for silicene as a function of E_z . \mathbf{B}^{in} and its anisotropy between z and x are very important for spin relaxation.

Spin relaxation under finite E_z . Spin lifetime, and even spin relaxation mechanism, can be tuned by applying electric fields.^{26,32} Under-

standing the effect of electric field is critical for the control and manipulation of spin relaxation. we start our theoretical studies of spin relaxation from its electric field dependence.

As we perform FPDM calculations of spin lifetimes in this work, it is important to understand the connection and distinction between FPDM method and previous theoretical models. Previously, spin relaxation mechanisms are often analyzed based on phenomenological models, such as Elliott–Yafet (EY) and D’yakonov-Perel’ (DP) mechanisms.³¹ EY represents the spin relaxation pathway due to spin-flip scattering. DP is activated when inversion symmetry is broken which results in random spin precession between adjacent scattering events. We denote their corresponding spin lifetime with τ_s^{EY} and τ_s^{DP} respectively. They are often approximated by some simplified relations:^{31,33,34} (i) $(\tau_{s,i}^{\text{EY}})^{-1} \approx 4 \langle b_i^2 \rangle \langle \tau_p^{-1} \rangle$ (EY relation) along direction i , where τ_p is carrier lifetime. $b_i^2 = 1 - 2S_i^{\text{exp}}$ is the degree of mixture of spin-up and spin-down states, so called ”spin mixing”^{31,35}, and is calculated at $E_z = 0$. (ii) $(\tau_{s,i}^{\text{DP}})^{-1} \approx \langle \tau_p^{-1} \rangle^{-1} \langle \Omega^2 - \Omega_i^2 \rangle$ (DP relation), where $\Omega_i = g_e \mu_B B_i^{\text{in}}$ is Larmor precession frequency³¹ with B_i^{in} defined earlier. Another qualitative estimation of the total spin relaxation rate by taking into account both mechanisms is using³⁶ $(\tau_s^{\text{E+D}})^{-1} = (\tau_s^{\text{EY}})^{-1} + (\tau_s^{\text{DP}})^{-1}$. In the following, we will compare FPDM calculations and these phenomenological models with first-principles input parameters including τ_p , b_i^2 and Ω_i .

We first investigate out-of-plane and in-plane spin lifetime $\tau_{s,z}$ and $\tau_{s,x}$, respectively, and their anisotropy ($\tau_{s,z}/\tau_{s,x}$) at $E_z = 0$ and 300K. From Fig.2 (a) and (b), we find that (i) $\tau_{s,z}$ and $\tau_{s,x}$ of silicene are much longer than germanene; (ii) large anisotropy (10-100) of τ_s is observed for both materials, e.g., 47 and 14 for silicene and germanene at zero E_z respectively, much greater than 0.5 for graphene^{7,26}. Both phenomena may be qualitatively understood based on EY relation (typically dominant in inversion symmetric systems) as discussed in the following. The comparison between FPDM calculations and EY relation with first-principles in-

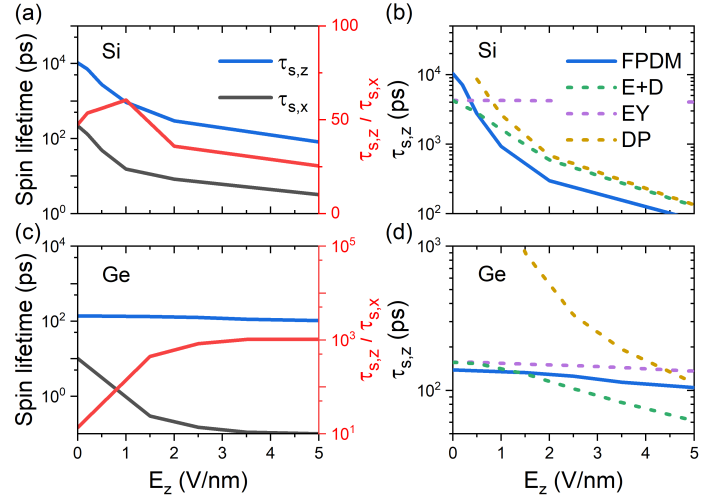


Figure 2: Spin lifetimes τ_s (left y -axis) and its anisotropy (right y -axis, red lines) of (a) intrinsic silicene and (c) intrinsic germanene as a function of E_z at 300 K. (b) and (d) are $\tau_{s,z}$ obtained by different methods of intrinsic silicene and germanene, respectively. “FPDM” - first-principles real-time density-matrix calculations. “EY” and “DP” correspond to $\tau_{s,z}^{\text{EY}}$ and $\tau_{s,z}^{\text{DP}}$ evaluated by EY and DP relations, respectively. “E+D” corresponds to $\tau_s^{\text{E+D}} = 1 / [1/\tau_s^{\text{EY}} + 1/\tau_s^{\text{DP}}]$.

puts is shown in Fig.2 (c) and (d), and they give the same order of magnitude of spin lifetime. Roughly speaking, the larger spin lifetime of silicene is mainly from the smaller spin mixing b^2 compared with germanene based on their intrinsic SOC strength. While the large spin anisotropy for both systems is a result of large ratio of b_z^2/b_x^2 (Fig. S6(a)).

We then discuss E_z dependence of spin relaxation. From Fig. 2(a) and 2(b), $\tau_{s,x}$ of silicene and germanene rapidly reduces with increasing E_z . This trend can be qualitatively understood as follows. Finite E_z breaks inversion symmetry and splits Kramers degeneracy. This induces \mathbf{B}^{in} with a rapidly increased z component as shown in Fig. 1(d), and thus leads to fast in-plane spin relaxation (perpendicular to B_z^{in}) and reduces in-plane spin lifetime $\tau_{s,x}$.

Unlike $\tau_{s,x}$, out-of-plane spin lifetime $\tau_{s,z}$ of germanene is insensitive to E_z in Fig. 2(c) although $\tau_{s,z}$ of silicene decreases fast with E_z (Fig. 2(a)). To better understand $\tau_{s,z}$ dependence on E_z , we compare FPDM $\tau_{s,z}$ with

the model calculations based on EY ($\tau_{s,z}^{\text{EY}}$), DP ($\tau_{s,z}^{\text{DP}}$) and EY+DP ($\tau_{s,z}^{\text{E+D}}$) mechanisms as introduced earlier, in Fig. 2(b) and 2(d). From Fig. 2(b) for silicene, we show that $\tau_{s,z}^{\text{E+D}}$ and $\tau_{s,z}^{\text{DP}}$ approximately agree with FPDM $\tau_{s,z}$ in trends. For germanene, however, from Fig. 2(d) we find that $\tau_{s,z}^{\text{EY}}$ is in good agreement with the FPDM $\tau_{s,z}$, but neither $\tau_{s,z}^{\text{E+D}}$ nor $\tau_{s,z}^{\text{DP}}$ capture the qualitative trend. Therefore, z -direction spin relaxation in germanene should be mostly driven by EY mechanism, insensitive to E_z . The suppression of DP mechanism in germanene under finite E_z may be due to the huge \mathbf{B}^{in} anisotropy $B_z^{\text{in}}/B_x^{\text{in}}$ (see Fig. 1(d) and Fig. S6(b)): as B_z^{in} is so strong, any in-plane spins will be quickly relaxed and all spins are pinned along z ; thus the total spin can only decay through direct spin-flip processes but not through spin precession driven by \mathbf{B}^{in} which changes spin direction gradually.

Temperature dependence of $\tau_{s,z}$ and spin-valley locking. It is important to understand the sensitivity of spin lifetime to temperature and determine the optimal operating temperature.^{30,38,39} Therefore, we show temperature dependence of $\tau_{s,z}$ without E_z and with $E_z = 2$ and 5 V/nm (higher than E_{cr} by ~ 2 V/nm) in intrinsic silicene and germanene respectively in Fig. 3(a) and (b). Without E_z , $\tau_{s,z}$ of both silicene and germanene increase fast on cooling. This is the usual behavior of EY spin lifetime simply due to weaker e-ph scattering with lowering temperature. Since phonon occupation is smaller at a lower temperature, τ_p is longer (Fig. S8), so τ_s is longer ($\tau_s \propto \tau_p$ with EY mechanism). Under finite E_z , $\tau_{s,z}$ of germanene are similar to the values under zero E_z as shown in Fig. 2(b), which are expected from the discussions on E_z dependence of germanene above. In sharp contrast, finite E_z significantly reduces $\tau_{s,z}$ of silicene and modifies the temperature dependence. To interpret such complex temperature dependence, in Fig. 3(c), we compare FPDM $\tau_{s,z}$ and the model ones $\tau_{s,z}^{\text{EY}}$, $\tau_{s,z}^{\text{DP}}$ and $\tau_{s,z}^{\text{E+D}}$ for silicene. All model relations fail to reproduce the temperature dependence under finite E_z for silicene. The failure of the DP relation in particular below 200 K is probably

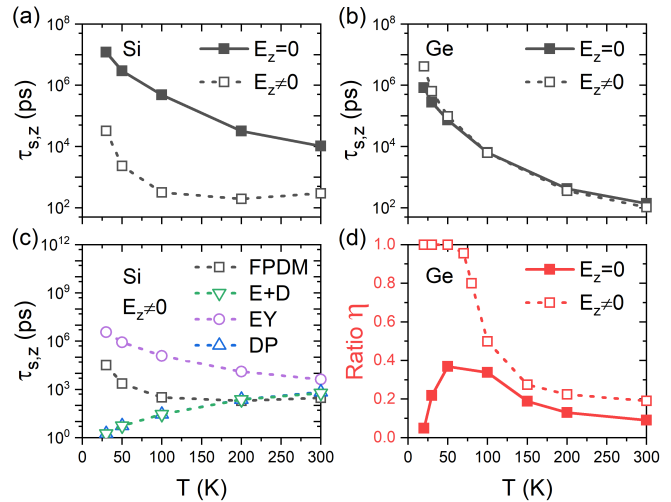


Figure 3: Temperature dependent $\tau_{s,z}$ of intrinsic (a) silicene and (b) germanene under $E_z = 0$ and $E_z \neq 0$ (2 and 5 V/nm for silicene and germanene, respectively). (c) $\tau_{s,z}$ of intrinsic silicene under $E_z \neq 0$ obtained by different methods. The labels of the curves have the same meanings as in Fig. 2. (d) Relative intervalley spin relaxation contribution η of germanene under $E_z = 0$ and $E_z \neq 0$. η is defined as $\eta = \frac{(\tau_{s,z}^{\text{inter}})^{-1}}{(\tau_{s,z}^{\text{inter}})^{-1} + w(\tau_{s,z}^{\text{intra}})^{-1}}$, where $\tau_{s,z}^{\text{inter}}$ and $\tau_{s,z}^{\text{intra}}$ are intervalley and intravalley spin lifetimes, corresponding to scattering processes between K and K' valleys and within a single K or K' valley, respectively. η being close to 1 or 0 corresponds to intervalley or intravalley scattering dominant spin relaxation, respectively. See more details of η in Ref. 37.

because it is inapplicable for weak scattering regime (weak e-ph scattering at low temperatures).³¹ Other relations have been proposed for weak scattering^{31,34,40}, e.g., $\tau_s \sim |\Omega|^{-1}$ and $\tau_s \sim 2\tau_p$, but none can capture the correct temperature dependence of $\tau_{s,z}$ of silicene under finite E_z , e.g., $\tau_s \sim |\Omega|^{-1}$ predicts $\tau_{s,z} < 20$ ps at all temperatures investigated here. Our theoretical studies highlight the importance of simulating spin lifetime using FPDM method for reliable prediction of spin lifetimes for large variations of external conditions.

Since the bands near the Fermi energy are composed of the Dirac cone electrons around K and K' valleys in silicene and germanene, spin relaxation process mostly arises from in-

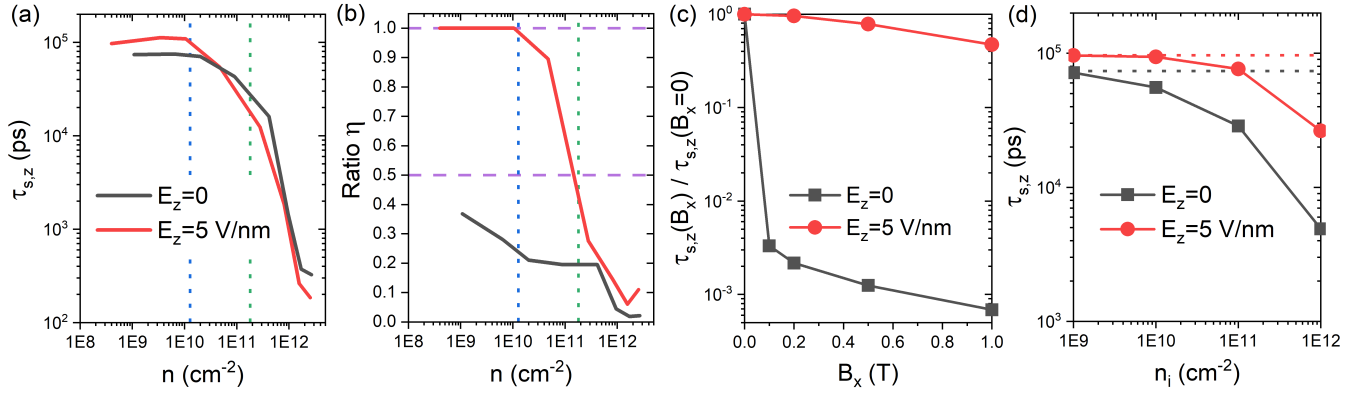


Figure 4: Spin relaxation in germanene at 50 K under 0 and 5 V/nm. (a) $\tau_{s,z}$ and (b) relative intervalley spin relaxation contribution η of germanene as a function of excess carrier density n , which is electron density n_e minus hole density n_h , and controlled by chemical potential μ . Positive carrier density corresponds to electron doping. (c) $\tau_{s,z}$ of germanene as a function of in-plane magnetic field - B_x . (d) $\tau_{s,z}$ of germanene as a function of impurity density n_i of neutral Ge vacancy (with n_e and n_h kept the same as intrinsic germanene). η being close to 1 or 0 correspond to spin relaxation being dominated by intervalley or intravalley scattering, respectively. The blue and green dotted vertical lines correspond to μ at the minima of first and second conduction bands respectively. The black and red dotted lines are $\tau_{s,z}$ in the zero n_i limit under $E_z = 0$ and 5 V/nm, respectively.

tervalley and intravalley scatterings. To scrutinize contributions of intervalley and intravalley scatterings to spin lifetime, we examine relative intervalley spin relaxation contribution η (see its definition in the caption of Fig. 3). η being close to 1 or 0 correspond to spin relaxation being dominated by intervalley or intravalley scattering, respectively. From Fig. 3(d), it is found that for germanene under $E_z=5$ V/nm, the η becomes close to 1 at $T \leq 70$ K. This indicates that under these conditions spin relaxation in germanene is dominated by intervalley process, which is a signature of so-called spin-valley locking. In addition, the long $\tau_{s,z}$ reaches around 100 ns at 50K and $E_z=5$ V/nm and indicates stability of spin states against spin relaxation. Different from germanene, in silicene, since the relatively small SOC splitting even at $E_z=2$ V/nm as shown in Fig. 1(b), the spin relaxation is mostly through intravalley scattering (not shown), which indicates silicene will hardly show the spin-valley locking property.

Formally the terminology “spin-valley locking” means that spin index (spin-up and spin-down) becomes locked with the valley index (e.g., K or K').⁴¹ This implies that (i) two val-

leys (e.g., K and K') exist with opposite spin polarizations. (ii) Within one valley, spins are all highly polarized along one direction, and carriers should have the same sign of spin. This needs large SOC splitting, i.e., the spin-up and down bands being largely separated.

Point (ii) will cause highly suppressed intravalley spin relaxation (i.e., relaxation through scattering processes within one valley). We explain the reason using germanene as an example: Under 5 V/nm, the SOC splitting for germanene is large, 23 meV at K . To have spins with the same sign, most of carriers should be located around the band edges (which require low temperatures and low carrier densities). Then the intravalley spin-flip transition between an occupied state at band edges and an empty state at the second conduction/valence band will be rather weak at relatively low temperatures, since phonon occupation becomes negligible at the corresponding phonon energy (comparable to SOC splitting).

On the other hand, for intervalley e-ph processes, the corresponding phonon wavevectors are away from Γ (e.g., around K) and the minimum phonon frequency is finite (e.g., 7 meV

for germanene, see Fig. S7). Therefore, with spin-valley locking, spin relaxation through e-ph scattering (mostly intervalley) will be highly suppressed leading to long spin lifetime, because of small phonon occupations at relatively low temperatures.

The existence of spin-valley locking not only leads to long spin lifetime but also allows the utilization of previously developed valleytronic technologies to design germanene-based devices^{1,3}. Our calculations provide guidance on the necessary conditions to realize spin-valley locking in germanene.

Carrier density and magnetic field dependence of $\tau_{s,z}$ for Germanene at low T. As intervalley scattering was shown being dominant in germanene at 50 K with a very long spin lifetime, we further investigate its spin relaxation as a function of carrier density, which can be easily tuned by electrical gate experimentally. We will also determine the range of carrier density where spin-valley locking happens.

As shown in Fig. 4(a), we plot $\tau_{s,z}$ of germanene as a function of excess carrier density n (which is electron density n_e minus hole density n_h , and controlled by chemical potential μ). We found it is very sensitive to n at the degenerate doping range ($n \gtrsim 4 \times 10^{10} \text{ cm}^{-2}$, corresponding to μ above the conduction band minimum). As the carriers contributing to spin relaxation have higher energies when n increases, the strong n dependence of $\tau_{s,z}$ should be mainly a result of the strength of the e-ph scattering being enhanced at higher energies (Fig. S10).

Moreover, we find that the relative intervalley spin relaxation contribution $\eta > 0.9$ at $n \leq 4 \times 10^{10} \text{ cm}^{-2}$ under $E_z = 5 \text{ V/nm}$ in Fig. 4(b). This indicates spin relaxation being dominated by intervalley processes and the presence of spin-valley locking at the corresponding condition, consistent with our above discussions about spin-valley locking.

We then investigate effects of spin-valley locking under in-plane magnetic-field B_x . From Fig. 4(c) at 50K for germanene, B_x has weak effects on spin lifetime of germanene under finite E_z . This is because the applied external

magnetic field is too weak compared with internal B field \mathbf{B}^{in} under finite E_z . This weak B_x dependence of spin lifetime is often used as an experimental evidence of spin-valley locking.¹⁰

Impurity effects and spin diffusion length.

Finally, we investigate the effects of the electron-impurity scattering. As an initial theoretical investigation, we will consider only one common neutral defect in germanene in this work - single Ge atom vacancy.⁴² From Fig. 4(d), we observe that $\tau_{s,z}$ are reduced by introducing impurities and the reduction becomes significant when impurity density n_i approaches 10^{12} cm^{-2} . Another interesting observation is that under finite $E_z = 5 \text{ V/nm}$, $\tau_{s,z}$ reduces much less than the one with $E_z = 0$. Our simulations suggest that if n_i can be controlled below 10^{12} cm^{-2} , especially under a finite E_z , germanene can exhibit long spin lifetime over 100 ns at or below 50 K.

At the end, we compute in-plane spin diffusion length l_{\parallel,s_z} for z -direction (out-of-plane) spin polarization of germanene using the relation³¹ $l_{\parallel,s_z} = \sqrt{D\tau_{s,z}}$, where D is diffusion coefficient. D can be estimated using the general form of Einstein relation⁴³ $D = \mu_c(n_e + n_h) / \frac{d(n_e + n_h)}{d\mu}$, where $\bar{\mu}_c$ is the average of electron and hole mobility, which are obtained from solving Boltzmann equation as detailed in the method section. From Table 1, we can see l_{\parallel,s_z} of germanene at 300 K is 2-3 μm , shorter than the longest measured value of graphene samples, $\sim 12 \mu\text{m}$.⁶ At 50 K, as mobilities are higher and $\tau_{s,z}$ are longer, l_{\parallel,s_z} become 400 μm without impurities and 120 μm with $n_i = 10^{11} \text{ cm}^{-2}$, which are much longer than experimental values of graphene at different temperatures ranging from 1 to 40 μm .⁹

Conclusions

By employing our newly developed first-principles density-matrix dynamics approach, we computed spin lifetime of two Dirac 2D materials - silicene and germanene as a function of temperature, electrical doping and neutral impurities, as well as applied electric and mag-

Table 1: Spin dynamic and transport properties of intrinsic germanene under $E_z=5$ V/nm without and with neutral impurities (with impurity density n_i). $\bar{\mu}_c$ is the average of electron and hole mobility. The method of calculating mobility is given in Supporting Information. The theoretical results of electron and hole mobility are given in Fig. S8. D is diffusion coefficient. l_{\parallel,s_z} is spin diffusion length of z -direction spin. The formula computing D and l_{\parallel,s_z} are given in the main text.

T (K)	n_i (cm $^{-2}$)	$\bar{\mu}_c$ (cm 2 /V/s)	D (cm 2 /s)	$\tau_{s,z}$ (ns)	l_{\parallel,s_z} (μ m)
300	0	3.2×10^4	830	0.1	2.9
300	10^{11}	2.5×10^4	620	0.1	2.5
50	0	3.8×10^6	16700	97	400
50	10^{11}	4.5×10^5	2000	76	120
50	10^{12}	5.8×10^4	250	26	25

netic fields. We find silicene and germanene have qualitative different spin relaxation mechanisms under finite E_z fields. We did systematic comparisons between our FPDM τ_s and those estimated by phenomenological models with first-principles input parameters. We find that germanene out-of-plane spin relaxation can be qualitatively understood by EY relation, regardless of the one with and without E field. On the other hand, spin relaxation in silicene is more complicated: although at room temperature, the trends of E_z dependence of silicene $\tau_{s,z}$ can be captured by a combination of EY and DP relation, the temperature dependence of $\tau_{s,z}$ under finite E_z cannot be explained by any simplified model relations.

We demonstrated giant spin lifetime anisotropy (two order of magnitude higher than graphene) and provided the condition for spin-valley locking with long spin lifetime in germanene. Specifically, we show that at a low T - 50 K, τ_s of germanene can reach 100 ns and l_s can exceed 100 μ m (longer than graphene samples), if impurity density is controlled low ($\leq 10^{11}$ cm $^{-2}$). This is very promising because the spin-valley locking property has only been realized in either TMDs which usually have much lower carrier mobility, or graphene on substrates which have complexity of interfacial engineering. The realization of spin-valley locking in single materials with long spin lifetime and ultrahigh mobility opens up highly promis-

ing pathways for spin-valleytronic applications.

Methods

To predict spin relaxation time from first principles, we employ our newly developed *ab initio* density-matrix dynamics approach, which includes quantum descriptions of various scattering processes and is applicable to general solid-state systems.^{29,30} The density matrix master equation due to the e-ph and e-i scattering in interaction picture reads:

$$\frac{d\rho_{12}(t)}{dt} = \frac{1}{2} \sum_{345} \left\{ \begin{array}{l} [I - \rho(t)]_{13} \rho_{45}(t) \times \\ [P_{32,45}^{e-ph}(t) + P_{32,45}^{e-i}(t)] \\ - [I - \rho(t)]_{45} \rho_{32}(t) \times \\ [P_{45,13}^{e-ph}(t) + P_{45,13}^{e-i}(t)]^* \end{array} \right\} + H.C., \quad (1)$$

where ρ is density matrix. H.C. is Hermitian conjugate. The subindex, e.g., “1” is the combined index of k-point and band. The weights of k points must be considered when doing sum over k points. P^{e-ph} and P^{e-i} are the generalized scattering-rate matrices for the e-ph and e-i scattering respectively. Note that P^c with c being a scattering channel is related to its value $P^{S,c}$ in the Schrodinger picture as $P_{1234}^c(t) = P_{1234}^{S,c} \exp[i(\varepsilon_1 - \varepsilon_2 - \varepsilon_3 + \varepsilon_4)t]$. $P^{S,c}$ is time independent and is computed from

corresponding e-ph or e-i matrix elements and electron and phonon energies.

All energies and matrix elements are calculated on coarse k and q meshes using the DFT software JDFTx,⁴⁴ and are then interpolated to extremely fine meshes in a basis of maximally localized Wannier functions.^{45–47} Starting from an initial state with a net spin, we evolve the density matrix $\rho(t)$ through the master equation Eq. 1 for a long enough simulation time, typically from ns to μ s. We then obtain the evolution of spin observable $S_i(t)$ ($i = x, y, z$) from $\rho(t)$ (Eq. S1). At the end, spin lifetime $\tau_{s,i}$ is obtained by fitting $S_i(t)$ to an exponential decay curve with decay constant $\tau_{s,i}$.

More details are given in Supporting Information Sec. SI and SII and Ref. 29.

Using the same first-principles electron and phonon energies and matrix elements on fine meshes, we calculate the carrier mobility by solving the linearized Boltzmann equation using a full-band relaxation-time approximation¹² (Supporting Information Sec. SVI).

Author contributions

J.X. and H.T. performed the *ab initio* calculations and analyses. R.S. and Y.P. designed and supervised all aspects of the study. All authors contribute to the writing of the manuscript.

Acknowledgements

We thank Mani Chandra for helpful discussions. This work is supported by the Air Force Office of Scientific Research under AFOSR Award No. FA9550-YR-1-XYZQ and National Science Foundation under grant No. DMR-1956015. A. H. acknowledges support from the American Association of University Women(AAUW) fellowship program. This research used resources of the Center for Functional Nanomaterials, which is a US DOE Office of Science Facility, and the Scientific Data and Computing center, a component of the Computational Science Initiative, at Brookhaven National Laboratory under Contract No. DE-SC0012704, the

lux supercomputer at UC Santa Cruz, funded by NSF MRI grant AST 1828315, the National Energy Research Scientific Computing Center (NERSC) a U.S. Department of Energy Office of Science User Facility operated under Contract No. DE-AC02-05CH11231, the Extreme Science and Engineering Discovery Environment (XSEDE) which is supported by National Science Foundation Grant No. ACI-1548562⁴⁸, and resources at the Center for Computational Innovations at Rensselaer Polytechnic Institute.

References

- (1) Schaibley, J. R.; Yu, H.; Clark, G.; Rivera, P.; Ross, J. S.; Seyler, K. L.; Yao, W.; Xu, X. Valleytronics in 2D materials. *Nat. Rev. Mater.* **2016**, *1*, 1–15.
- (2) Zhang, L.; Gong, K.; Chen, J.; Liu, L.; Zhu, Y.; Xiao, D.; Guo, H. Generation and transport of valley-polarized current in transition-metal dichalcogenides. *Phys. Rev. B* **2014**, *90*, 195428.
- (3) Tao, L.; Naeemi, A.; Tsymbal, E. Y. Valley-spin logic gates. *Phys. Rev. Appl.* **2020**, *13*, 054043.
- (4) Han, W.; Kawakami, R. K.; Gmitra, M.; Fabian, J. Graphene spintronics. *Nat. Nanotechnol.* **2014**, *9*, 794–807.
- (5) Das Sarma, S.; Adam, S.; Hwang, E. H.; Rossi, E. Electronic transport in two-dimensional graphene. *Rev. Mod. Phys.* **2011**, *83*, 407–470.
- (6) Drogeler, M.; Franzen, C.; Volmer, F.; Pohlmann, T.; Banszerus, L.; Wolter, M.; Watanabe, K.; Taniguchi, T.; Stampfer, C.; Beschoten, B. Spin lifetimes exceeding 12 ns in graphene nonlocal spin valve devices. *Nano Lett.* **2016**, *16*, 3533–3539.
- (7) Cummings, A. W.; Garcia, J. H.; Fabian, J.; Roche, S. Giant Spin Lifetime Anisotropy in Graphene Induced by Proximity Effects. *Phys. Rev. Lett.* **2017**, *119*, 206601.

- (8) Gmitra, M.; Fabian, J. Proximity Effects in Bilayer Graphene on Monolayer WSe₂: Field-Effect Spin Valley Locking, Spin-Orbit Valve, and Spin Transistor. *Phys. Rev. Lett.* **2017**, *119*, 146401.
- (9) Avsar, A.; Ochoa, H.; Guinea, F.; Özyilmaz, B.; van Wees, B. J.; Vera-Marun, I. J. Colloquium: Spintronics in Graphene and Other Two-Dimensional Materials. *Rev. Mod. Phys.* **2020**, *92*, 021003.
- (10) Dey, P.; Yang, L.; Robert, C.; Wang, G.; Urbaszek, B.; Marie, X.; Crooker, S. A. Gate-Controlled Spin-Valley Locking of Resident Carriers in WSe₂ Monolayers. *Phys. Rev. Lett.* **2017**, *119*, 137401.
- (11) Cheng, L.; Liu, Y. What limits the intrinsic mobility of electrons and holes in two dimensional metal dichalcogenides? *J. Am. Chem. Soc.* **2018**, *140*, 17895–17900.
- (12) Ciccarino, C. J.; Christensen, T.; Sundararaman, R.; Narang, P. Dynamics and spin-valley locking effects in monolayer transition metal dichalcogenides. *Nano Lett.* **2018**, *18*, 5709–5715.
- (13) Ezawa, M. Valley-polarized metals and quantum anomalous Hall effect in silicene. *Phys. Rev. Lett.* **2012**, *109*, 055502.
- (14) Tsai, W.-F.; Huang, C.-Y.; Chang, T.-R.; Lin, H.; Jeng, H.-T.; Bansil, A. Gated silicene as a tunable source of nearly 100% spin-polarized electrons. *Nat. Commun.* **2013**, *4*, 1–6.
- (15) Dávila, M. E.; Xian, L.; Cahangirov, S.; Rubio, A.; Le Lay, G. Germanene: a novel two-dimensional germanium allotrope akin to graphene and silicene. *New J. Phys.* **2014**, *16*, 095002.
- (16) Zhang, L.; Bampoulis, P.; Rudenko, A.; Yao, Q. v.; Van Houselt, A.; Poelsema, B.; Katsnelson, M.; Zandvliet, H. Structural and electronic properties of germanene on MoS₂. *Phys. Rev. Lett.* **2016**, *116*, 256804.
- (17) Zhao, J.; Liu, H.; Yu, Z.; Quhe, R.; Zhou, S.; Wang, Y.; Liu, C. C.; Zhong, H.; Han, N.; Lu, J.; et al., Rise of silicene: A competitive 2D material. *Prog. Mater. Sci.* **2016**, *83*, 24–151.
- (18) Shao, Z.-G.; Ye, X.-S.; Yang, L.; Wang, C.-L. First-principles calculation of intrinsic carrier mobility of silicene. *J. Appl. Phys.* **2013**, *114*, 093712.
- (19) Ye, X.-S.; Shao, Z.-G.; Zhao, H.; Yang, L.; Wang, C.-L. Intrinsic carrier mobility of germanene is larger than graphene's: first-principle calculations. *RSC Adv.* **2014**, *4*, 21216–21220.
- (20) Liu, C.-C.; Feng, W.; Yao, Y. Quantum Spin Hall Effect in Silicene and Two-Dimensional Germanium. *Phys. Rev. Lett.* **2011**, *107*, 076802.
- (21) Acun, A.; Zhang, L.; Bampoulis, P.; Farmanbar, M.; van Houselt, A.; Rudenko, A. N.; Lingenfelder, M.; Brocks, G.; Poelsema, B.; Katsnelson, M. I.; Zandvliet, H. J. W. Germanene: the germanium analogue of graphene. *J. Phys. Condens. Matter* **2015**, *27*, 443002.
- (22) Han, W.; Kawakami, R. K. Spin relaxation in single-layer and bilayer graphene. *Phys. Rev. Lett.* **2011**, *107*, 047207.
- (23) Kamalakar, M. V.; Groenveld, C.; Dankert, A.; Dash, S. P. Long distance spin communication in chemical vapour deposited graphene. *Nat. Commun.* **2015**, *6*, 1–8.
- (24) Restrepo, O. D.; Windl, W. Full first-principles theory of spin relaxation in group-IV materials. *Phys. Rev. Lett.* **2012**, *109*, 166604.
- (25) Cummings, A. W.; Roche, S. Effects of dephasing on spin lifetime in ballistic spin-orbit materials. *Phys. Rev. Lett.* **2016**, *116*, 086602.

- (26) Habib, A.; Xu, J.; Ping, Y.; Sundararaman, R. Electric Field and Substrate Effects Dominate Spin-Phonon Relaxation in Graphene. *arXiv preprint arXiv:2012.11550* **2020**,
- (27) Bishnoi, B.; Ghosh, B. Spin transport in silicene and germanene. *RSC Adv.* **2013**, *3*, 26153–26159.
- (28) Babaei Touski, S. Spin transport in armchair silicene nanoribbon on the substrate: The role of charged impurity. *Phys. Status Solidi B* **2019**, *256*, 1900082.
- (29) Xu, J.; Habib, A.; Sundararaman, R.; Ping, Y. Ab initio Ultrafast Spin Dynamics in Solids. *arXiv preprint arXiv:2012.08711* **2020**,
- (30) Xu, J.; Habib, A.; Kumar, S.; Wu, F.; Sundararaman, R.; Ping, Y. Spin-Phonon Relaxation from a Universal Ab Initio Density-Matrix Approach. *Nat. Commun.* **2020**, *11*, 2780.
- (31) Žutić, I.; Fabian, J.; Sarma, S. D. Spintronics: Fundamentals and Applications. *Rev. Mod. Phys.* **2004**, *76*, 323.
- (32) Guimarães, M. H.; Zomer, P. J.; Inglis, J.; Brant, J. C.; Tombros, N.; van Wees, B. J. Controlling spin relaxation in hexagonal BN-encapsulated graphene with a transverse electric field. *Phys. Rev. Lett.* **2014**, *113*, 086602.
- (33) Fabian, J.; Sarma, S. D. Spin relaxation of conduction electrons in polyvalent metals: Theory and a realistic calculation. *Phys. Rev. Lett.* **1998**, *81*, 5624.
- (34) Leyland, W.; Harley, R.; Henini, M.; Shields, A.; Farrer, I.; Ritchie, D. Oscillatory Dyakonov-Perel spin dynamics in two-dimensional electron gases. *Phys. Rev. B* **2007**, *76*, 195305.
- (35) Kurpas, M.; Junior, P. E. F.; Gmitra, M.; Fabian, J. Spin-orbit coupling in elemental two-dimensional materials. *Phys. Rev. B* **2019**, *100*, 125422.
- (36) Bronold, F. X.; Martin, I.; Saxena, A.; Smith, D. L. Magnetic-field dependence of electron spin relaxation in n-type semiconductors. *Phys. Rev. B* **2002**, *66*, 233206.
- (37) w is a weight factor related to how many percent of total S_z can be relaxed out by intravalley scattering itself. w being close to 0 and 1 correspond to intravalley scattering can only relax a small part and most of excess spin respectively. In Supporting Information Sec. SVIII and Fig. S11, we give more details about w .
- (38) Yang, L.; Sinitsyn, N. A.; Chen, W.; Yuan, J.; Zhang, J.; Lou, J.; Crooker, S. A. Long-Lived Nanosecond Spin Relaxation and Spin Coherence of Electrons in Monolayer MoS₂ and WS₂. *Nat. Phys.* **2015**, *11*, 830–834.
- (39) Kikkawa, J. M.; Awschalom, D. D. Resonant Spin Amplification in n-Type GaAs. *Phys. Rev. Lett.* **1998**, *80*, 4313.
- (40) Wu, M.; Jiang, J.; Weng, M. Spin dynamics in semiconductors. *Phys. Rep.* **2010**, *493*, 61–236.
- (41) Xu, X.; Yao, W.; Xiao, D.; Heinz, T. F. Spin and pseudospins in layered transition metal dichalcogenides. *Nat. Phys.* **2014**, *10*, 343–350.
- (42) Hastuti, D. P.; Nurwantoro, P., et al. Stability study of germanene vacancies: The first-principles calculations. *Mater. Today Commun.* **2019**, *19*, 459–463.
- (43) Kubo, R. The fluctuation-dissipation theorem. *Rep. Prog. Phys.* **1966**, *29*, 255.
- (44) Sundararaman, R.; Letchworth-Weaver, K.; Schwarz, K. A.; Gunceler, D.; Ozhobes, Y.; Arias, T. A. JDFTx: Software for Joint Density-Functional Theory. *SoftwareX* **2017**, *6*, 278–284.
- (45) Marzari, N.; Vanderbilt, D. Maximally Localized Generalized Wannier Functions for Composite Energy Bands. *Phys. Rev. B* **1997**, *56*, 12847.

- (46) Brown, A. M.; Sundararaman, R.; Narang, P.; Goddard, W. A.; Atwater, H. A. Nonradiative Plasmon Decay and Hot Carrier Dynamics: Effects of Phonons, Surfaces, and Geometry. *ACS Nano* **2016**, *10*, 957–966.
- (47) Habib, A.; Florio, R.; Sundararaman, R. Hot Carrier Dynamics in Plasmonic Transition Metal Nitrides. *J. Opt.* **2018**, *20*, 064001.
- (48) Towns, J.; Cockerill, T.; Dahan, M.; Foster, I.; Gaither, K.; Grimshaw, A.; Hazelwood, V.; Lathrop, S.; Lifka, D.; Peterson, G. D.; Roskies, R.; Scott, J. R.; Wilkins-Diehr, N. XSEDE: Accelerating Scientific Discovery. *Comput. Sci. Eng.* **2014**, *16*, 62–74.